NRIM SR-94-02

Dynamic Fracture Toughness and Its Evaluation in a Heavy-Sectioned Ferritic Nodular Cast Iron

by

Takashi YASUNAKA

NRIM Special Report
(Research Report)
No. 94–02

1994

National Research Institute for Metals
2–3–12, Nakameguro, Meguro-ku, Tokyo, Japan

NRIM SR-94-02

Dynamic Fracture Toughness and Its Evaluation in a Heavy-Sectioned Ferritic Nodular Cast Iron

by

Takashi YASUNAKA

NRIM Special Report
(Research Report)
No. 94-02

1994

National Research Institute for Metals
2-3-12, Nakameguro, Meguro-ku, Tokyo, Japan

Dynamic Fracture Toughness and Its Evaluation in a Heavy-Sectioned Ferritic Nodular Cast Iron

by
Takashi YASUNAKA

NRIM Special Report
(Research Report)
No. 94–02

Contents

Dynamic Fracture Toughness and Its Evaluation in a Heavy-Sectioned Ferritic Nodular Cast Iron

by

Takashi YASUNAKA*

Abstract

Recently, heavy-sectioned ferritic nodular cast iron has become to be made and the use of this material is noticed. Ferritic nodular cast iron, however, has low toughness because it contains a large amount of graphite. Furthermore, embrittlement occurs at low temperature. Therefore, to use this material for large structural components, the evaluation of upper shelf fracture toughness as well as ductile-brittle transition temperature is necessary.

Static fracture toughness increases with increase in internodule spacing, whereas dependence of dynamic fracture toughness on internodule spacing is small. The upper shelf fracture toughness increases with decrease in temperature and with increase in stress intensity rate. This increase in fracture toughness is mainly attributed to the increase in strength. Fracture toughness transition temperature is linearly related to the logarithm of stress intensity rate.

In the upper shelf region, plane strain fracture toughness divided by yield stress is constant, and it is proposed as a material constant that is independent of stress intensity rate and temperature. Evaluation of the critical flaw size for unstable fracture can be simplified with this fracture toughness parameter.

Keywords: *ferritic nodular cast iron, dynamic fracture toughness, low temperature embrittlement, stress intensity rate, graphite internodule spacing, structural integrity*

* Senior Researcher, Environmental Performance Division, NRIM

1. Introduction

1.1 Objective of This Study

Ferritic nodular cast iron has great fluidity, little shrinkage and good machinability in comparison with cast steel, and has been developed as a material for a ductile cast iron. One of the disadvantages of this material is low toughness because of large amount of graphite. Furthermore, embrittlement occurs at low temperature. This embrittlement was studied by impact testing such as Charpy impact testing. Afterward, fracture mechanics became to be applied to the evaluation of the toughness of this material, and the effect of metallurgical factors on fracture toughness has been studied[1].

Because the control of cooling rate is required in the process of production, thickness of castings was limited in the early stages. However, heavy-sectioned castings have become to be made, and they are used as large structural components[2]. In recent years, from the viewpoint of economy, the nuclear spent fuel shipping cask of ferritic nodular cast iron, which also serves as an intermediate storage cask, has attracted particular attention and has been developed in Germany[3]. Such casks have been also developed in Japan, and thick-walled ferritic nodular cast iron castings have become to be produced[4–6]. The Japan Industrial Standard of thick-walled ferritic nodular cast iron castings for low temperature service (JIS FCD 300 LT) has been established[7]. For the application to casks, it is required to evaluate dynamic fracture toughness for preventing unstable fracture against impact load at low temperatures.

In the case of thick-walled ferritic nodular cast iron castings, the microstructure varies with the location of wall thickness. The mid-thickness portion of castings at which final solidification occurs has large graphite nodules because of low cooling rate. The mid-thickness portion is often inferior to the other portion in strength and elongation[5], and is regarded as the weakest portion of castings. It is inconsistent, however, with the data reported previously on the fracture toughness of the mid-thickness portion of castings. It is worthwhile to clarify the effect of graphite distribution on fracture toughness because the results relate to the sampling of test coupons and the method of quality assurance. Furthermore, it is preferable to estimate fracture toughness using small specimens because of the different microstructures depending on the location in castings.

Objectives of this study are to characterize the behavior of fracture toughness with respect to graphite distribution and loading rate and to evaluate fracture toughness of this material.

1.2 Historical Review

1.2.1. Static Fracture Toughness and Specimen Thickness

In the early period, the measurements of plane strain fracture toughness were attempted on the basis of linear elastic fracture mechanics. These attempts were not successful except at low temperature where brittle fracture occurred.

Nanstad et al.[8–11] measured plane strain fracture toughness K_{IC} of ferritic nodular cast irons using the compact tension (CT) specimens of 21 mm in thickness, but valid K_{IC} value was not obtained. They regarded K_Q or K_{max} that was calculated from the 5% secant load or the maximum load, respectively, as fracture toughness.

In the upper shelf region, it was difficult to obtain valid K_{IC} even if the specimen with large thickness was used. Ostensson[12] used CT specimen of 100 mm in thickness and reported that K_{IC} was not valid. Recently, Arai et al.[13] found that valid K_{IC} was not obtained in the upper self region even with CT specimens of 200 mm in thickness.

In the upper shelf region, therefore, elastic-plastic fracture toughness J_{IC} was measured. Here, K_{IC} estimated from J_{IC} is termed $K_{IC}(J)$. Bradley and Mead, Jr.[14] measured J_{IC} at room temperature using CT specimens. They obtained $K_{IC}(J)$ of 41 to 54 $MPam^{1/2}$. Another $K_{IC}(J)$ of 25 to 67 $MPam^{1/2}$ was reported by Bradley[15].

1.2.2. Chemical Composition

Effect of the amount of carbon on critical crack opening displacement (COD) was studied by Holdsworth and Jolley[16]. Increase in volume fraction of graphite led to a decrease in critical COD value in the upper shelf region and to reduction in COD transition temperature.

Bradley and Mead, Jr.[14] found that J_{IC} of nodular cast iron containing 3% Si was small under some temperature conditions. Maezono et al.[17] showed that J_{IC} increased with increasing the amount of Si in the range

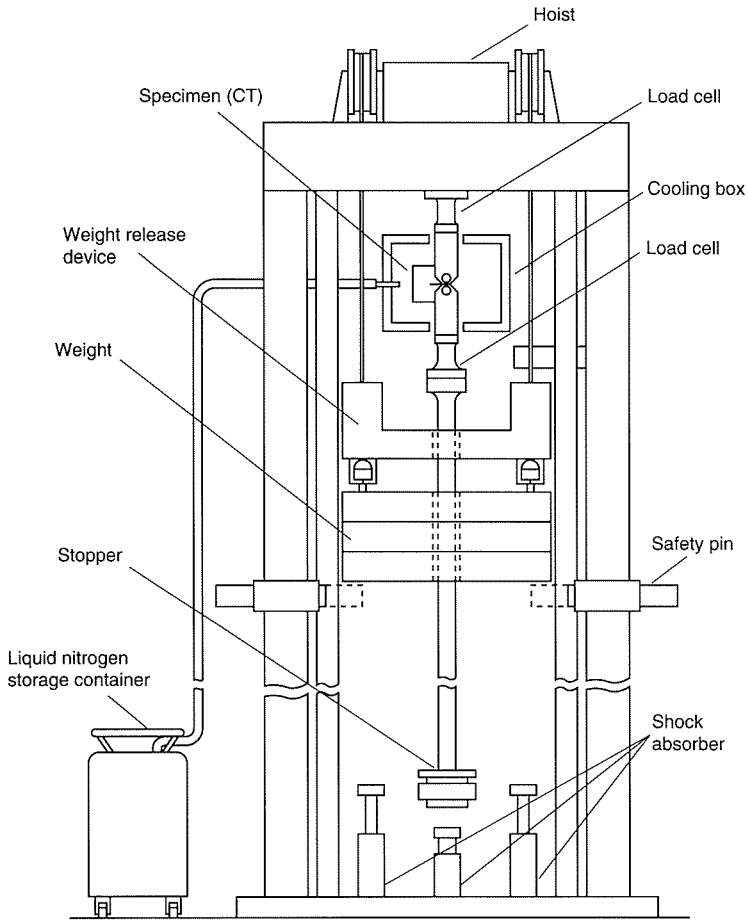

Fig. 1 Schematic illustration of the drop-weight testing machine

from 1.87 to 3.12% but decreased when the amount of Si was beyond this range. Komatsu et al.[18] studied the effect of the amount of Si on J_{IC}. They found that J_{IC} in the upper shelf region increased with increasing the amount of Si up to 2.9%, and further increase in the amount of Si led to a decrease in J_{IC}. On the other hand, at 123 K in the lower shelf region J_{IC} decreased with increasing the amount of Si. Ductile-brittle transition temperature of J_{IC} was lowered with increasing the amount of Si.

Komatsu et al.[19] showed that the resistance to crack propagation decreased with increasing the amount of P and the amount of P above 0.05% resulted in rapid increase in the ductile-brittle transition temperature. However, in the upper shelf region a little decrease in J_{IC} was observed with increase in the amount of P. Moreover, Krasowsky et al.[20] reported that K_{IC} decreased with increasing the amount of Mn.

1.2.3. Pearlite

Matrix is composed of ferrite, pearlite or mixture of the two phases. Kobayashi[21] showed that J_{IC} increased when the amount of pearlite was less than 10%. Bradley and Mead, Jr.[14] also obtained the similar conclusion. Transition temperature increased with increase in the amount of pearlite[22]. It was confirmed by Komatsu et al.[23] that J_{IC} at room temperature decreased with increasing volume fraction of pearlite up to 92% and transition temperature increased. Krasowsky et al.[20] also reported that K_{IC} decreased as pearlite percentage increased.

1.2.4. Graphite Nodularity

Kuribayashi et al.[24] studied the effect of graphite nodularity using the samples with nodularity up to 84%. They showed that J_{IC} increased with increasing nodularity, and the relationship between nodularity n and J_{IC} was

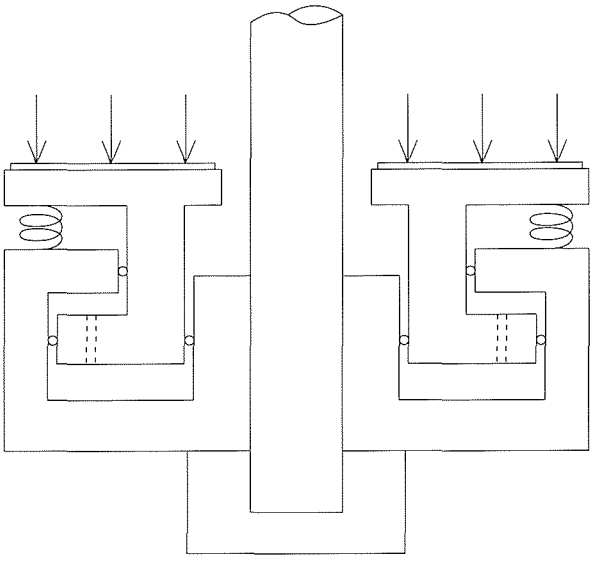

Fig. 2 Stopper having an inner oil damper

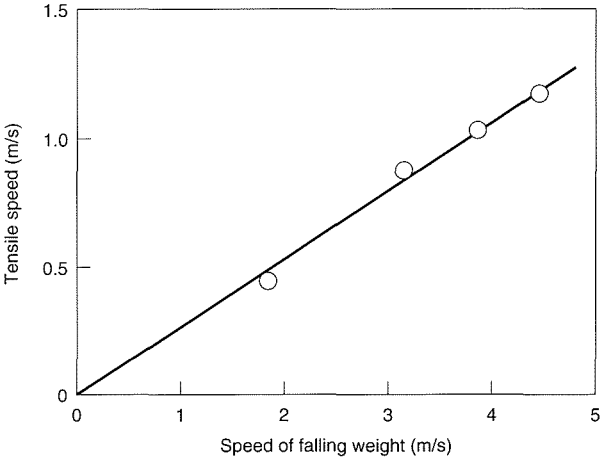

Fig. 3 Relationship between tensile speed and speed of falling weight

represented by the following equation:

$$J_{IC} = 62 - 14.7\left(n^{-1/2} - n^{3/2}\right) \quad \left(kJm^{-2}\right) \ldots\ (1)$$

Komatsu et al.[25] also reported that J_{IC} in the upper shelf region increased with increasing nodularity.

1.2.5. Internodule Spacing and Nodule Size of Graphite

Holdsworth and Jolley[16] showed the effect of nodule count on COD when the amount of carbon was constant. Increase in nodule count, that is, decrease in internodule spacing reduced COD value in the upper shelf region and reduced slightly COD transition temperature. Sorenson and Salzbrenner[26] showed using many data that K_Q increased with increase in internodule spacing and nodule size. Maezono et al.[27] carried out the fracture toughness tests using 3 point bend specimens. They reported that J_{IC} in the upper shelf region increased, but J_{IC} in the brittle fracture region decreased with increasing graphite nodule size. Salzbrenner[28] found large dependence of J_{IC} on internodule spacing or nodule size.

Regarding ferritic nodular cast iron for thick-walled castings, Iwabuchi et al.[29] reported that fracture toughness increased with increasing nodule size. However, Nakamura et al.[4] found that J_{IC} at the mid-thickness portion where final solidification occurred was smaller in magnitude than that at the other portions.

1.2.6. Dynamic Fracture Toughness

Measurement of dynamic plane strain fracture toughness K_{Id} by dynamic tear test was made by Cheng and Worzala[11] and a shift of K_{Id}-temperature curve to higher temperature was shown. Kobayashi and Nishi[30] reported the characteristics of fracture including K_{Id}. Luyendijk and Nieswaag[31] measured dynamic fracture toughness using an instrumented Charpy testing machine. They found little variation in fracture toughness at the impact speed from 2.2 to 5.4 ms^{-1}. Kobayashi et al.[32] made the instrumented Charpy impact test using fatigue precracked specimens taken from thick-walled ferritic nodular cast iron castings. They revealed the effect of specimen size and the behavior of $K_{Id}(J)$. Transition temperature of $K_{Id}(J)$ at the impact speed of 1.34 ms^{-1} was about 90 K lower than that of $K_{IC}(J)$.

Loading rate in the instrumented Charpy test has been represented by the impact speed of the hammer. Behavior of fracture may depend on strain rate in the region adjacent to the crack tip. Therefore, stress intensity rate (dK/dt or $\dot{K}$) is preferable for loading rate.

Quality assurance committee on ductile cast iron casks (1986 to 1990) was organized by Central Research Institute of Electric Power Industry in Japan. The thick-walled castings of ferritic nodular cast iron were supplied by several casting manufacturers, and characteristics of these materials were studied. Dynamic fracture toughness

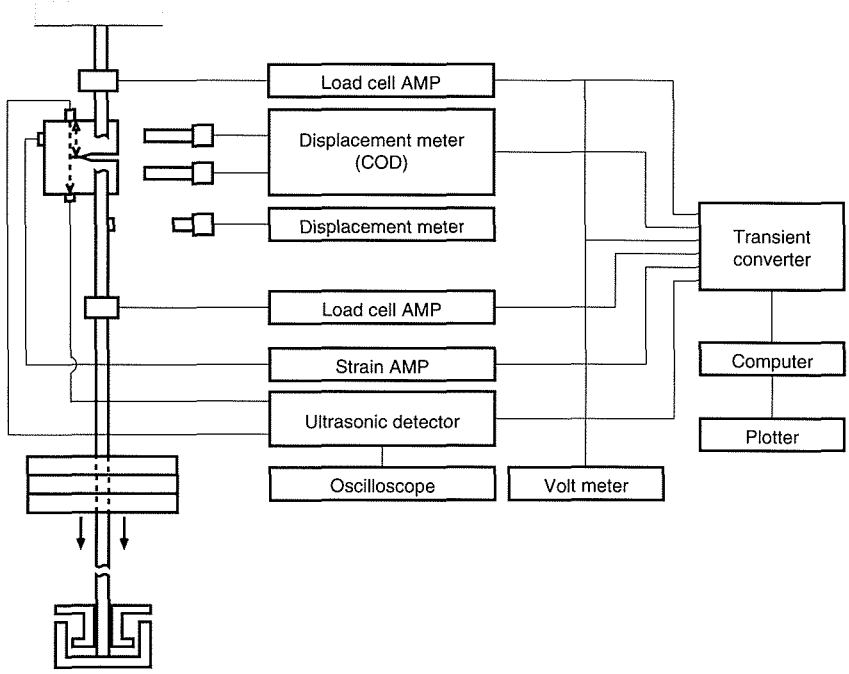

Fig. 4 Block diagram of measuring system

was measured using CT specimens up to 150 mm in thickness and the level of fracture toughness values was confirmed[33].

2. Development of a Drop-weight Impact Testing Machine[47]

For the measurement of dynamic fracture toughness, many kinds of testing machines, such as hydraulic and gas-actuated tensile machine[34], pendulum-type impact machine[35], drop-weight testing machine[36, 37], and split Hopkinson-bar[38], have been used.

Although the drop-weight testing machine has a disadvantage of relatively narrow range of loading rate, it has many advantages in economy, operation, and maintenance by virtue of the simple structure. Mostly, it has been used as an impact bending machine[36, 37]. It, however, would be available as an impact tensile testing machine. For measuring dynamic fracture toughness, an impact tensile machine with a falling weight was designed and made.

Figure 1 shows schematically the specially designed testing machine. A loading rod is suspended under the CT specimen. A stopper is mounted at the lower end of the loading rod. In this study, the weight of 200 kg was used. The weight is lifted to a predetermined height by a hoist and then released. Impact test is made by forcing down the loading rod by the free falling weight. The specimens can be automatically cooled in a cooling box and held at a predetermined temperature by fine spray of liquid nitrogen. Specimens are shielded from liquid nitrogen by shielding plate. Two load cells are installed above and below the specimen.

In the case of iron block stopper, the tensile speed was ascertained to be equivalent to the falling speed of the weight. Dropping the weight from the height that exerted enough energy to fracture the specimen led to the occurrence of elastic waves. The data obtained were not able to be treated similarly as those in static test. Furthermore, time lag of the output of transducers became large. The stopper that had an inner oil damper as shown in Fig. 2 was used to dampen the initial shock wave and to obtain lower tensile speed. The relationship between calculated falling speed of weight and tensile speed is shown in Fig. 3.

The block diagram of the measuring system is shown in Fig. 4. For the measurement of COD, the displacement between two targets marked on the front face of the CT specimen was measured by an electro-optical displace-

Table 1 Chemical composition (wt%)

Material	C	Si	Mn	P	S	Mg
A	3.56	2.02	0.18	0.019	0.002	0.04
B	3.56	2.00	0.18	0.019	0.002	0.04
C	3.56	2.04	0.19	0.002	0.002	0.04

ment meter. Tensile speed was measured from the displacement of a light-emitting diode located at the upper end of the loading rod, using an optical displacement meter. The data were stored into a transient converter and saved on floppy disks and then analyzed with a computer.

3. Experimental Procedure

3.1 Materials[50]

Test materials were taken from an as-cast cylindrical casting of 500 mm in wall thickness and 1350 mm in outside diameter. The casting was cut into many 60 × 125 × 150 mm^3 blocks. The test blocks from 15, 30 and 45% thick position in the direction to the inner surface are denoted as Materials A, B and C, respectively. In those materials, the graphite distributions differ each other due to different cooling rates.

The chemical compositions are listed in Table 1. There was little difference between the chemical compositions of Materials A, B and C. Microstructures are shown in Photo. 1. The graphite nodularity was high and little pearlite was observed. Graphite nodule size increased and nodule count decreased in the sequence of Materials A, B and C. The grain size in Material C was a little large in comparison with the others. Graphite nodule diameter was measured with an image analyzer; each area of graphite was converted to the corresponding diameter of circle. Figure 5 shows the distribution of graphite nodule on a test plane. Metallographic details such as graphite nodule and grain size are listed in Table 2. The definition of interparticle spacing depends on interaction between a particle and the phenomenon under consideration. Figure 6 shows the relationship between the angle just ahead of the precrack tip and the expected value of distance ξ_A from the precrack tip to the center of the nearest neighbors of nodules within the angle. We use $N_A^{-1/2}$ as a parameter of internodule spacing.

3.2 Mechanical Property Testing

Tensile specimens with a diameter of 4 mm and a gage length of 20 mm were tested in an Instron machine and a high rate tensile testing machine. Impact tests were carried out on the standard V-notched Charpy specimens and on the bend specimens with machine notch of 0.06 mm in root radius and of 2 mm in notch depth instead of V notch.

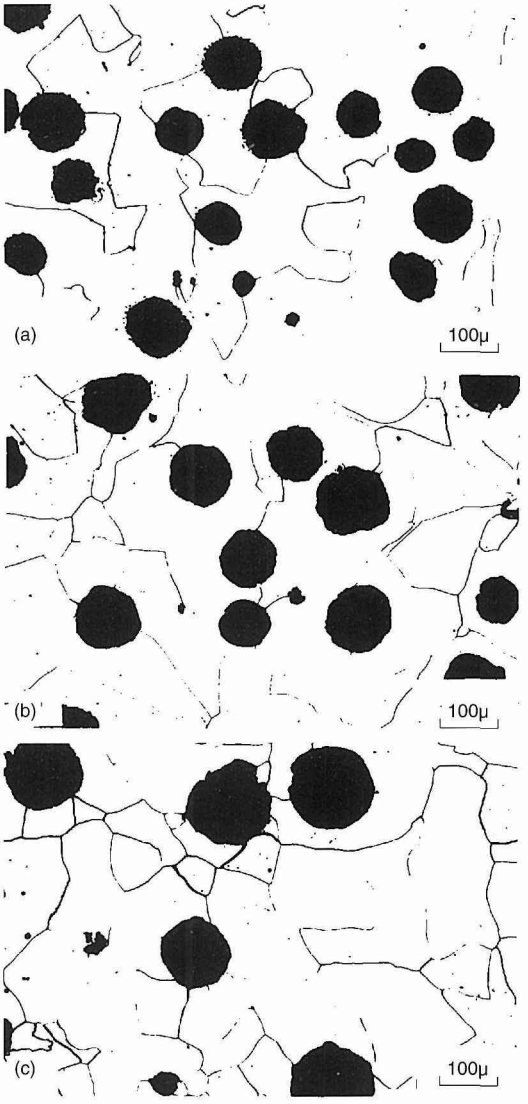

Photo. 1 Optical microstructures of Materials A (a), B (b) and C (c)

3.3 Fracture Toughness Testing[48, 49]

Static and dynamic elastic-plastic fracture toughness, J_{IC} and J_{Id}, respectively, were measured by the multiple-specimen and single-specimen techniques according to ASTM E813-81 or JSME S 001. The specimens were fatigue precracked CT specimens of 25 mm in thickness as shown in Fig. 7. The testing machines used were the

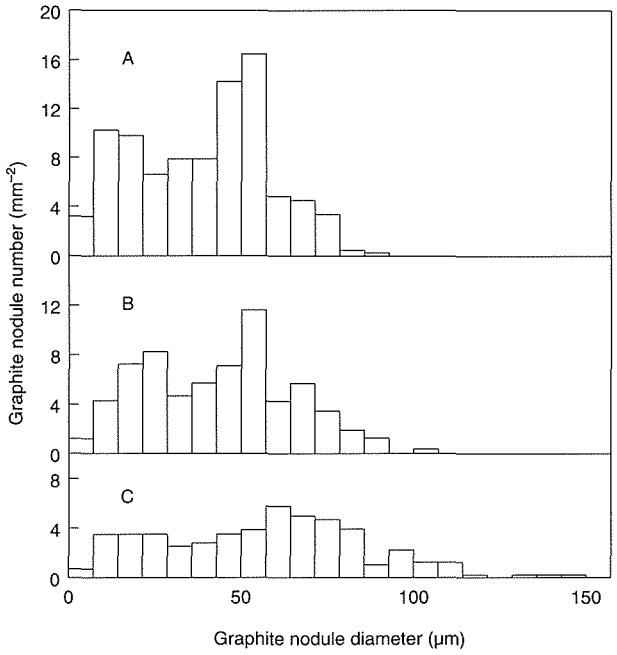

Fig. 5 Distribution of graphite nodule diameter on a test plane

Table 2 Metallographic details

Material	A	B	C
Graphite nodule number N_A (mm^{-2})	90.6	67.2	49.5
Mean graphite diameter on a test plane (mm)	0.0391	0.0443	0.0513
Mean graphite diameter in volume (mm)	0.0479	0.0542	0.0628
Internodule spacing parameter $N_A^{-1/2}$ (mm)	0.105	0.122	0.142
Degree of nodularity (%)	98	97	98
Grain size number	5.6	5.1	4.7

drop-weight type, an electrohydraulic type and Instron tensile ones.

To detect the onset of crack propagation in dynamic test, the ultrasonic method[39] used in static tests is noteworthy though electrical potential method[40] and caustics method[41] are often used. An ultrasonic method was applied in this study. Ultrasonic method makes it possible to detect the onset of crack propagation in the mid-thickness portion of several square millimeter in area where the crack can be propagated most easily in the specimen. As shown in Fig. 8 two disks of piezoelectric ceramics were cemented at the location that corresponded to the crack tip on the upper and lower faces of the

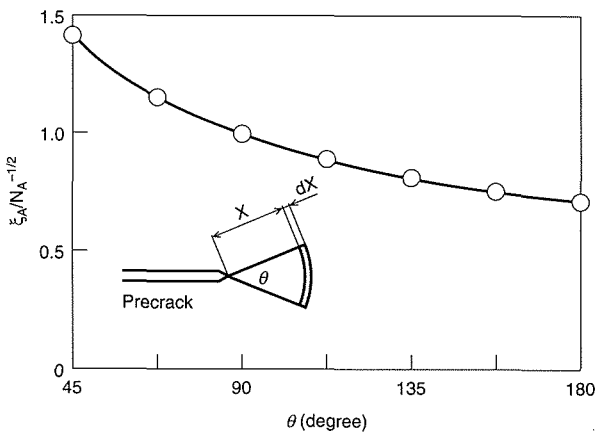

Fig. 6 Relationship between angle near the precrack tip and distance from the precrack tip to the nearest neighbor graphite nodule found within its angle

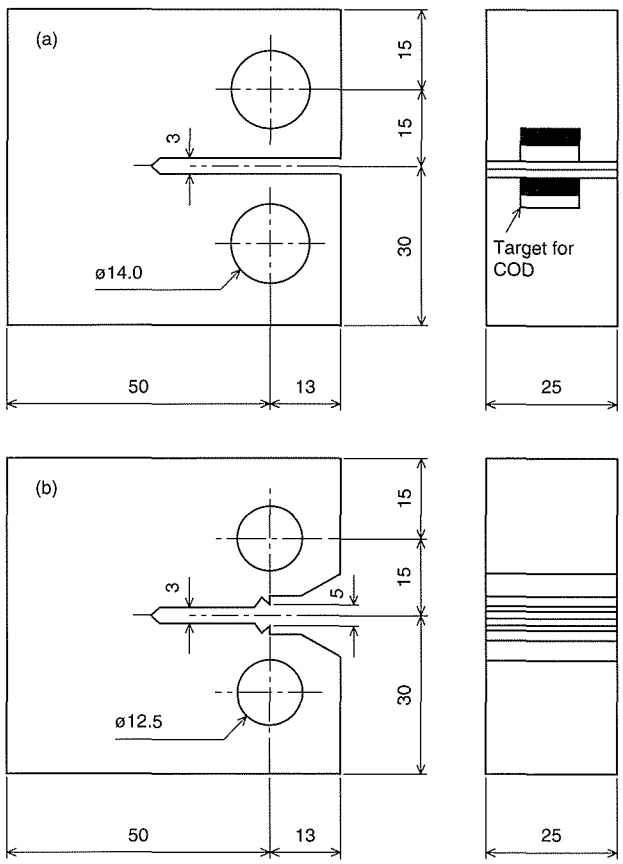

Fig. 7 Configurations of the compact tension specimens for a drop-weight type tensile machine (a), electrohydraulic type and Instron tensile machines (b).

specimen. Variation in ultrasonic reflection and through transmission pulse heights was measured. Figure 9 shows

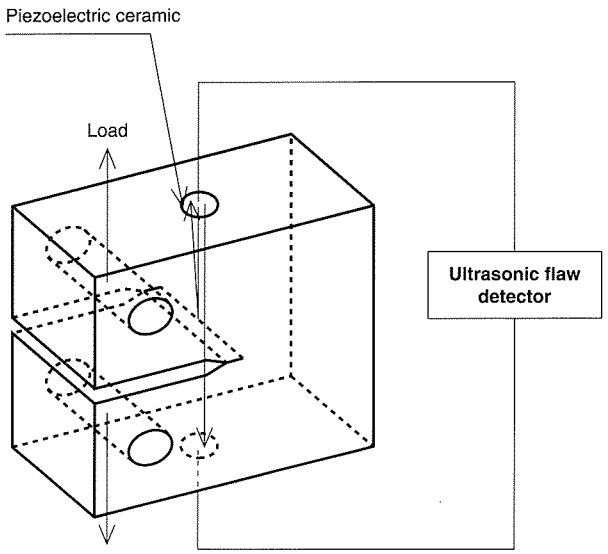

Fig. 8 Schematic illustration of measuring the onset of crack propagation by an ultrasonic method

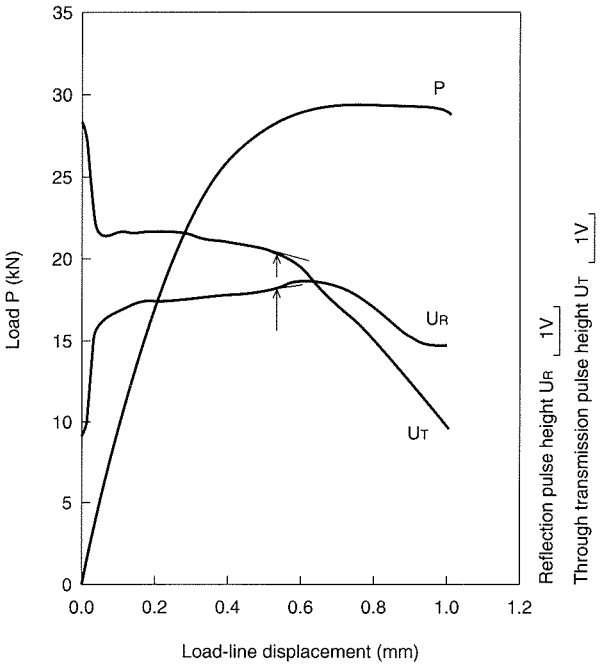

Fig. 9 Typical variation in load and ultrasonic pulse height showing the onset of crack propagation by the arrows under static test in an Instron machine

typical changes in pulse height under static test. The onset of crack propagation is shown by the arrows. The similar change under dynamic test in the drop-weight type testing machine is shown in Fig. 10. Reflection method was effective in this case. Reflection pulse height began to increase at the moment of impact. This was followed by another abrupt and discontinuous change with crack propagation. The onset of crack propagation occurred before reaching the maximum load.

In the range of tensile speed below 1 ms^{-1}, the load measured by the upper load cell was in good agreement with that estimated by back-face strain. Therefore, J_{Id} can be calculated by the following equation[42] applied in static test:

$$J_{IC},\ J_{Id} = Af(a/w)/(Bb) \quad \cdots\cdots (2)$$

where A is the area under load and load-line displacement record, a is the precrack length, b is the initial uncracked ligament, W is the width of specimen, B is the thickness of specimen, and

$$f(a/W) = 2(1+\alpha)/\left(1+\alpha^2\right)$$
$$\alpha = \left\{(2a/b)^2 + 2(2a/b) + 2\right\}^{1/2} - \left\{(2a/b)+1\right\} \quad \cdots (3)$$

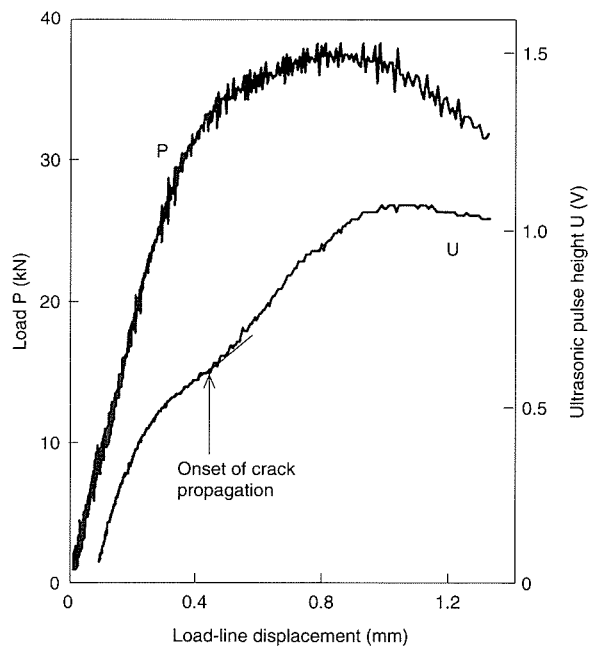

Fig. 10 Typical variation in load and ultrasonic reflection pulse height showing the onset of crack propagation by the arrow under dynamic test in a drop-weight type tensile machine

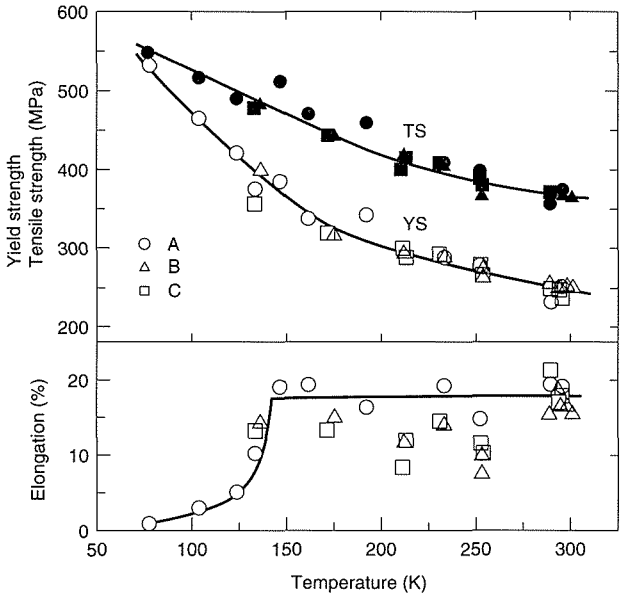

Fig. 11 Effect of temperature on tensile properties

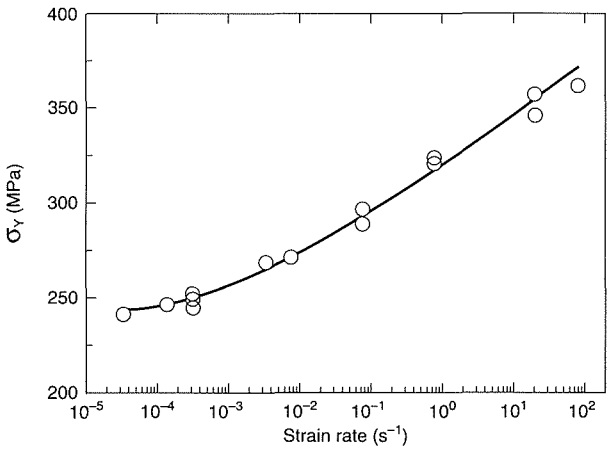

Fig. 12 Effect of strain rate on yield strength at room temperature, Material A

4. Mechanical Properties[49, 51]

4.1 Tensile and Charpy Impact Properties

The effect of temperature on tensile properties is shown in Fig. 11. Strength was insensitive to graphite distribution. Figure 12 shows the dependence of 0.2% proof yield strength on strain rate at room temperature. The result of V-notch Charpy impact test is shown in Fig. 13. The absorbed energy in the upper shelf region was 17 J and the absorbed energy transition temperature was 253 K. The data indicate a small scatter even in the transition region.

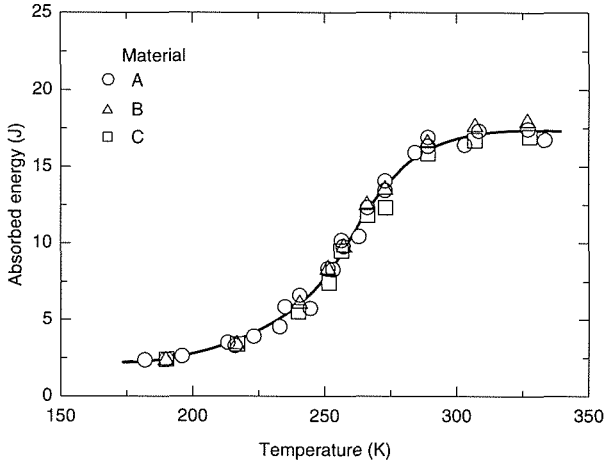

Fig. 13 Charphy V-notch impact energy curve

4.2 Young's Modulus

Young's modulus E can be calculated from the compliance C of CT specimen by the following equation[43]:

$$E = (1/CB)\{(W+a)/(W-a)\}^2 \begin{Bmatrix} 2.1630 + 12.219(a/W) - 20.065(a/W)^2 \\ -0.9925(a/W)^3 + 20.609(a/W)^4 \\ -9.9314(a/W)5 \end{Bmatrix} \quad (4)$$

The results are illustrated by Fig. 14. Relationship between Young's modulus E and temperature T (K) was represented by the following equation:

$$E = 196.5 - 0.066\,T \quad \text{(GPa)} \quad \cdots\cdots\cdots\cdots \quad (5)$$

5. Fracture Toughness[49-51]

5.1 Effect of Internodule Spacing

Figure 15 shows the J-R curves obtained by static fracture toughness tests at room temperature. In these specimens tested, stretched zone was not observed, and crack blunting line was not able to be measured clearly. Therefore, the intercept between the regression line and the crack blunting line given by the equation $J = 2\sigma_f \Delta a$ was identified as J_{IC}. Here, σ_f is the effective yield

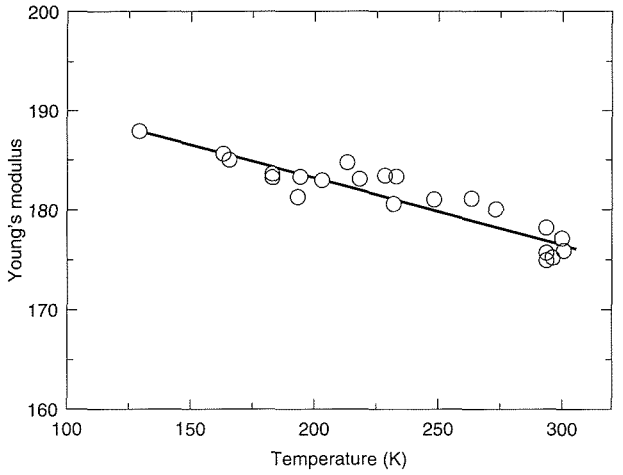

Fig. 14 Young's modulus as a function of temperature, Material A.

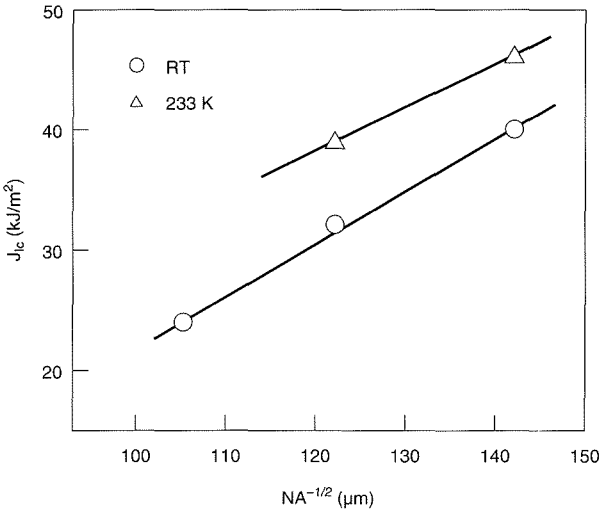

Fig. 16 Relationship between J_{IC} and $N_A^{-1/2}$ at room temperature and 233 K, Material A

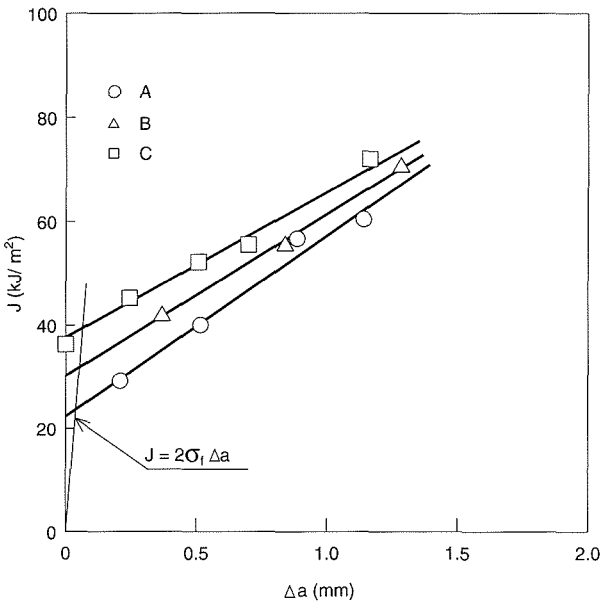

Fig. 15 J-R curve under static test at room temperature, initial stress intensity rate of 0.42 MPam$^{1/2}$s^{-1}

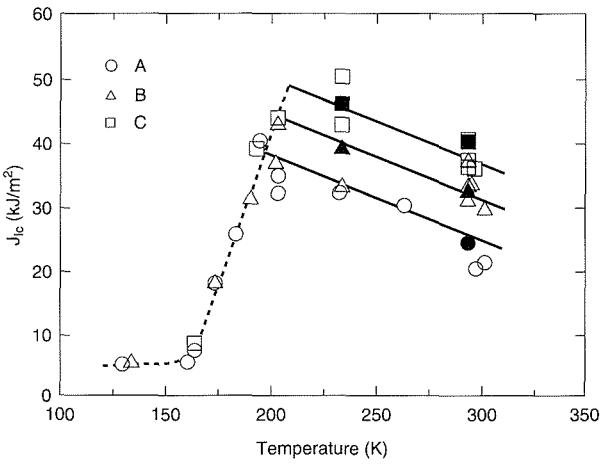

Fig. 17 Effect of temperature and graphite distribution on J_{IC}

strength and Δa is the increment of crack length. The J_{IC} increased in the sequence of Materials A, B and C; J_{IC} was influenced by graphite distribution. The relationship between parameter of internodule spacing and J_{IC} in the upper shelf region is shown in Fig. 16. Fracture toughness J_{IC} increased with increasing parameter of internodule spacing.

The effect of temperature on J_{IC} is shown in Fig. 17. The data plotted by the solid symbols in the figure indicate those obtained by the multiple-specimen technique. Upper shelf region existed until temperature decreased to about 200 K. In the upper shelf region, in which fracture appearance was ductile one, J_{IC} increased with decreasing temperature. Further decrease in temperature led to an increase in cleavage fracture resulting in decrease in J_{IC}; J_{IC} decreased with increase in percentage of brittle fracture appearance. At early stage, cleavage fracture surface of the order of one grain size was isolated each other. In the ductile-brittle transition region, difference between J_{IC} values in Materials A, B and C was not observed. This may be attributed to little difference in grain size. Transition temperature was 188 K. Crack propagation in the upper shelf region occurred

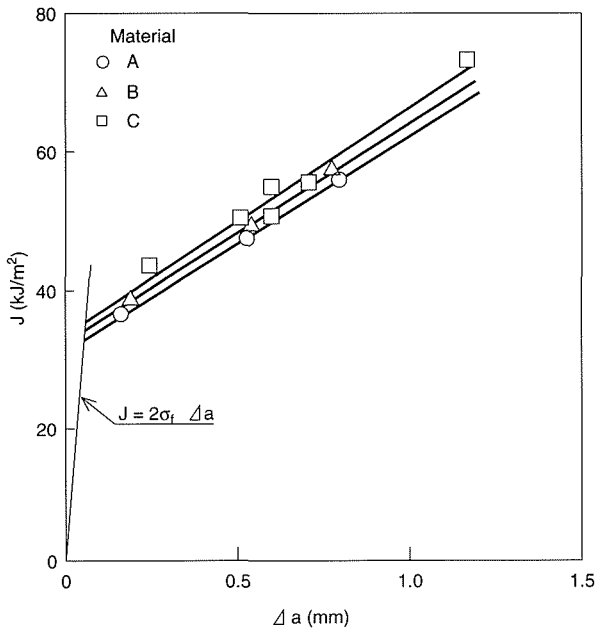

Fig. 18 J-R curve under dynamic test at room temperature, initial stress intensity rate of 6.7 $MPam^{1/2}s^{-1}$

predominantly by void growth around graphite nodule and coalescence.

Figure 18 shows the J-R curves at dK/dt of 6.7 $MPam^{1/2}s^{-1}$. Dynamic elastic-plastic fracture toughness J_{Id} was influenced to a less extent by graphite nodule spacing. In the case of larger dK/dt, experimental accuracy was reduced, so that the difference between J_{Id} values of Materials A, B and C was not found experimentally.

5.2 Effect of Stress Intensity Rate

The effect of dK/dt on fracture toughness is shown in Fig. 19. Upper shelf fracture toughness was increased with increasing dK/dt. Ductile-brittle transition temperature was naturally raised with increasing dK/dt. Dependence of fracture toughness and critical crack tip opening displacement on dK/dt is demonstrated in Fig. 20. Within this range of dK/dt, specimens were fractured in ductile mode at room temperature. Upper shelf fracture toughness was linearly related to the logarithm of dK/dt. Crack tip opening displacement (CTOD) can be calculated from the following equation specified by British standard[44]:

$$\mathrm{CTOD} = K^2(1-\nu^2)/2\sigma_Y E + 0.46(W-a)V_p/(0.46W+0.54a) \quad \cdots (6)$$

where K is the stress intensity factor, σ_Y is the yield

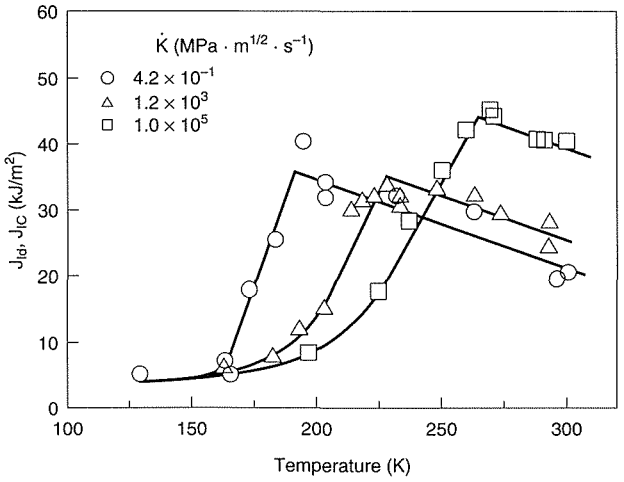

Fig. 19 Variation in fracture toughness as a function of temperature with various stress intensity rates

strength, ν is Poisson's ratio, and V_P is the plastic component of load-line displacement. The second term of the right side of this equation is the plastic component of CTOD and is denoted by $CTOD_{plastic}$ distinguishing it from total CTOD ($CTOD_{total}$). Especially, the dependence of $CTOD_{plastic}$ on dK/dt was small. Therefore, the increase in fracture toughness with increasing dK/dt is mainly attributed to the increase in strength.

The effect of dK/dt on transition temperature is shown in Fig. 21. There was a linear relation between the transition temperature and the logarithm of dK/dt. In addition, it should be noted that the transition temperature of this material was equivalent to that of a low carbon steel.

5.3 Fracture Toughness Parameter

Plane strain fracture toughness divided by yield strength as a function of temperature is shown in Fig. 22. Static and dynamic plane strain fracture toughness, $K_{IC}(J)$ and $K_{Id}(J)$ were estimated from J_{IC} and J_{Id}, respectively. The K values were converted by the following equation:

$$K = \{EJ/(1-\nu^2)\}^{1/2} \quad \cdots (7)$$

Yield strength was estimated using the equation of nominal limit load of CT specimen[43] on the assumption of constant yield ratio. In the upper shelf region, $K_{IC}(J)/\sigma_Y$ and $K_{Id}(J)/\sigma_Y$ were kept constant regardless of tempera-

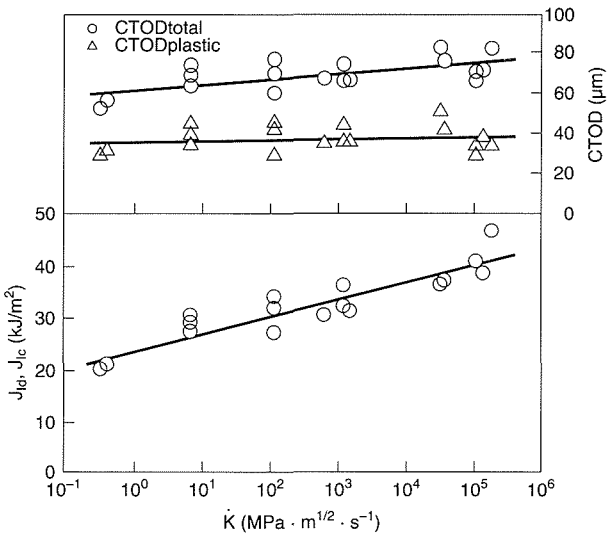

Fig. 20 Effect of stress intensity rate on fracture toughness and CTOD at room temperature in the upper shelf region

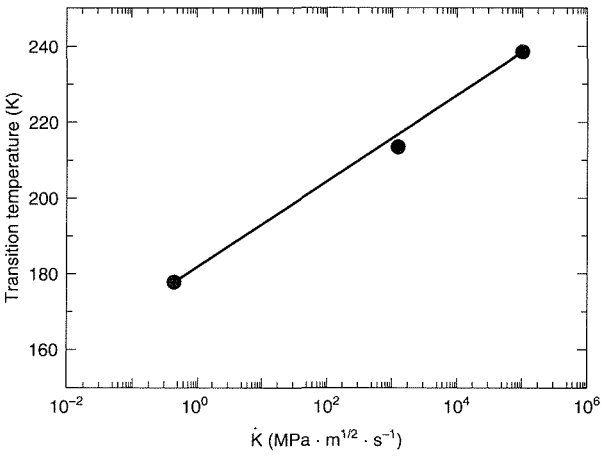

Fig. 21 Effect of stress intensity rate on fracture toughness transition temperature

ture and dK/dt. This fracture toughness parameter may be regarded as a material constant of this material.

5.4 Estimation of Fracture Toughness from Small Size Specimen

There are various difficulties in measuring dynamic fracture toughness of ferritic nodular cast irons. It is preferable to estimate the behavior of fracture toughness at the predetermined dK/dt from the results of static fracture toughness tests and impact tests of small specimens. The results of an impact bend test using small

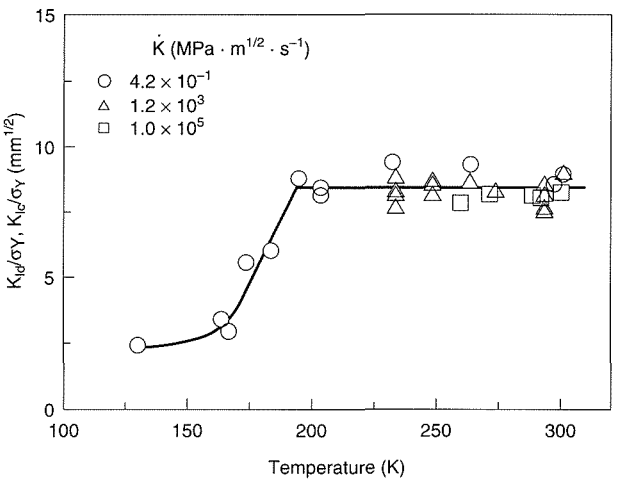

Fig. 22 Fracture toughness normalized to yield strength as a function of temperature with various stress intensity rates

specimens with machined notches are shown in Fig. 23. The dK/dt in the impact test can be estimated from the impact speed and the dK/dt in a static bend test. When the root radius of machined notch is in the same order of magnitude as internodule spacing, the sharpness of machined notch may be equivalent to that of fatigue-cracked notch because of the existence of graphite nodule. In such a case, the estimation of the behavior of fracture toughness might be possible through percentage of brittle fracture appearance in front of the precrack tip.

In this study, increase in percentage of brittle fracture appearance of more than 50% led to rapid decrease in J_{Id}. The conditions of 50% brittle fracture appearance corresponded to that of the lower limit of temperature in the upper shelf region. It was found that the temperature at the beginning of embrittlement in fracture toughness and the corresponding temperature of 50% brittle fracture appearance in CT or machine-notched specimens were linearly related to the logarithm of dK/dt.

Figure 24 shows a method to estimate the behavior of fracture toughness at the predetermined dK/dt. Point A is obtained by static test using CT specimens, whereas Point B is obtained by impact test using small bend specimens with machined notches. In the figure, T_I is the lowest temperature of upper shelf region and T_s is the 50% brittle fracture transition temperature. Point D is determined from Point C that corresponds to the predetermined dK/dt on the line AB. Thus, the relationship between K_{Id}/σ_Y and temperature can be estimated.

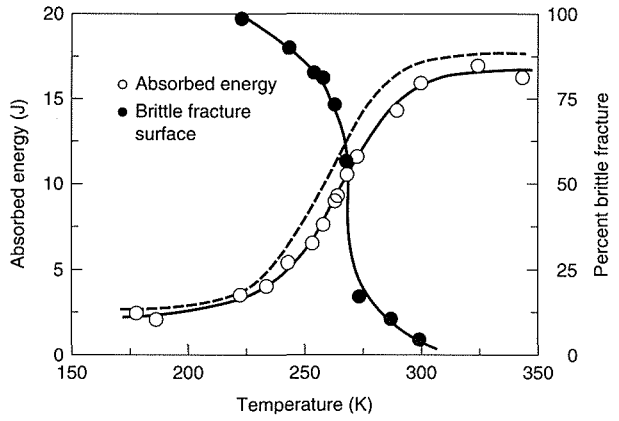

Fig. 23 Impact energy and percentage of brittle fracture appearance of the machine-notched bend specimen as a function of temperature. The broken line shows Charpy V-notch impact energy curve.

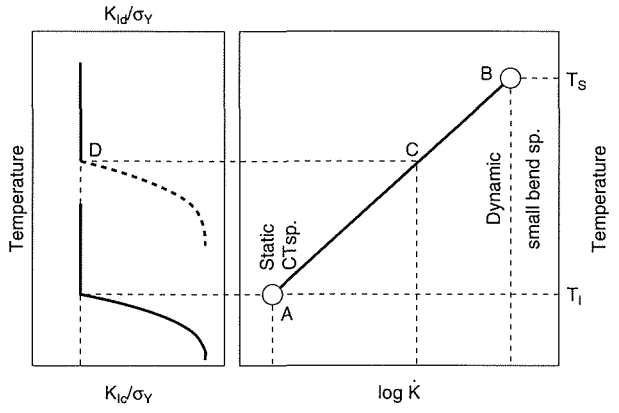

Fig. 24 Estimation of dynamic fracture toughness behavior by static fracture toughness tests and impact tests with small machine-notched bend specimen

6. Evaluation of Fracture Toughness[51, 52]

In the ferritic nodular cast iron, it is necessary to evaluate upper shelf fracture toughness for preventing unstable fracture in the upper shelf region as well as ductile-brittle transition temperature. An attempt has been made to recommend the design criterion by the conventional method on the basis of strength and static fracture toughness[45]. The resistance of crack propagation in this material is relatively small. It is difficult to establish the Pellini-type fracture toughness reference curve because of the difficulties in measuring nil ductility transition temperature by dynamic tear test. Within the limited range of dK/dt, the reference curve relating to K_{Id} and relative temperature may be established. In general, however, the prediction of unstable fracture on the basis of crack initiation criterion seems to be reasonable. Here, the analysis based on linear elastic fracture mechanics is employed.

Variation in $K_{Id}(J)$ with temperature is shown in Fig. 25. The shaded area in the figure shows the range of fracture toughness values reported by Arai et al.[26] In the region shown by a lighter shade, plane strain fracture toughness was valid. On the other hand, in the region shown by a darker shade, namely, in the upper shelf region, plane strain fracture toughness was invalid regardless of using CT specimens of 150 and 200 mm in thickness. The upper shelf fracture toughness in this study was smaller than that reported by Arai et al. The critical allowable flaw size can be calculated by these data. Analysis of unstable fracture, however, can be simplified by the above-mentioned fracture toughness parameter.

For example, it is assumed that a semi-elliptical surface crack exists perpendicular to the surface of thick plate as shown in Fig. 26. A load that is superimposed by tension and bending is applied to the plate. The stress intensity factor becomes maximum value at Point A under the condition described later. There are many papers that give the calculation of the stress intensity factor in such a case. According to Ishida et al.[45], the stress intensity factor at Point A is represented by the following equation:

$$K = (\pi b)^{1/2}(\sigma_M F_M + \sigma_B F_B) \quad \cdots\cdots (8)$$

where both F_M and F_B are the functions of b/a and b/t, which are given by polynomials. The total stress on the surface of plate is expressed by:

$$\sigma = \sigma_M + \sigma_B \quad \cdots\cdots (9)$$

When $\sigma_B/\sigma_M = \beta$, the stress intensity factor is given by:

$$K = \sigma_M(\pi b)^{1/2}(F_M + \beta F_B) \quad \cdots\cdots (10)$$

Relationship between stress on the plate surface and

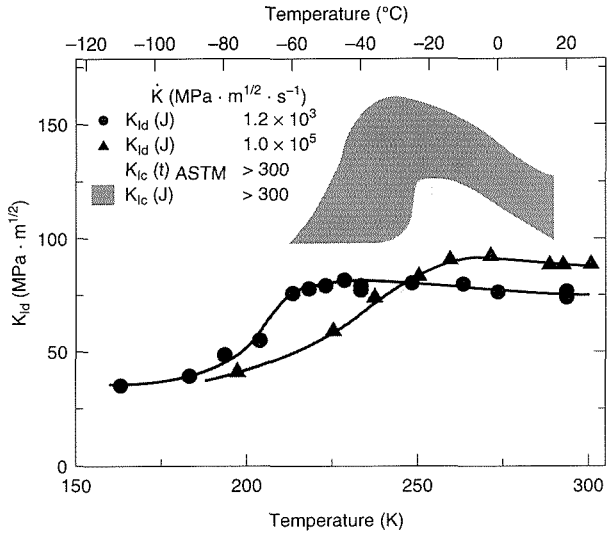

Fig. 25 Dynamic plane strain fracture toughness as a function of temperature

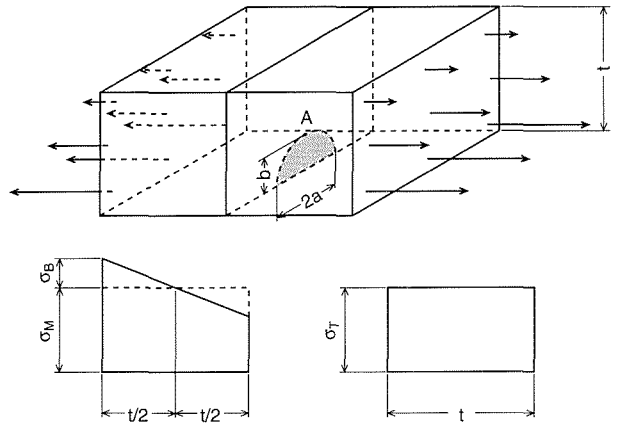

Fig. 26 Tension and bending of a finite-thickness plate with a semi-elliptical surface crack

critical depth of surface flaw b_C can be determined from:

$$\sigma/\sigma_Y = (K_{Id}/\sigma_Y)(1+\beta)\Big/\left\{(\pi b_C)^{1/2}(F_M + \beta F_B)\right\} \qquad (11)$$

Here, b/a and t are assumed to be 1/4 and 400 mm, respectively. In the upper shelf region of this material, $K_{Id}(J)/\sigma_Y$ is regarded as a constant as mentioned before. When stress on the plate surface is constant, uniform tension (β=0) results in the minimum value of critical flaw depth. Relationship between stress under uniform tension σ_T and critical flaw depth $b_{C(T)}$ is shown in Fig. 27. The solid line in the figure shows the relation for the material used in this study. If σ is constant, the critical flaw depth $b_{C(M,B)}$ increases with increasing bending stress σ_B. Relationship between σ_B/σ_M and $b_{C(M,B)}/b_{C(T)}$ is shown in Fig. 28.

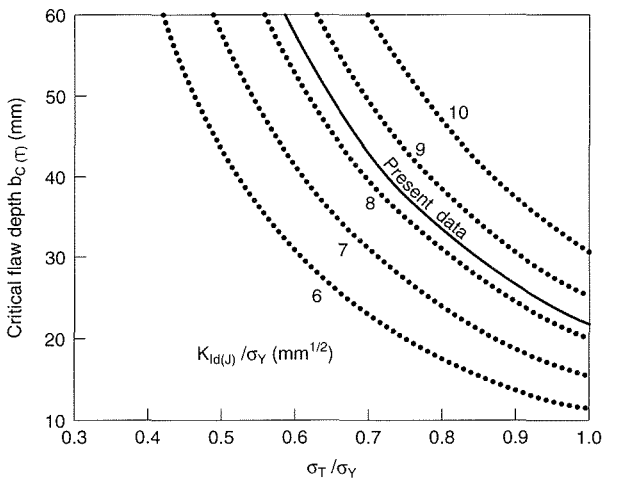

Fig. 27 Critical surface flaw depth as a function of uniform tensile stress in the upper shelf region with normalized fracture toughness

7. Concluding Remarks

Heavy-sectioned castings of ferritic nodular cast iron have become to be produced recently, and this material has attracted particular attention as an economic one. Toughness of this material is relatively low because of large amount of graphite. Careful evaluation of toughness, therefore, is necessary in the use of this material. However, little systematic study of dynamic fracture toughness has been made. In the production of castings of this material, relatively much know-how is required, and this enables manufacturers to produce castings with somewhat different quality. The microstructure of ferrite nodular cast iron used in this study was excellent one having low volume fraction of pearlite and high nodularity. Behavior of fracture toughness in regard to temperature and loading rate has been studied. In this study, elastic-plastic fracture toughness was adopted as fracture toughness because plane strain fracture toughness was probably not effective in the upper shelf region even if thick specimens were used.

Embrittlement occurred at low temperature and fracture toughness transition temperature was linearly related

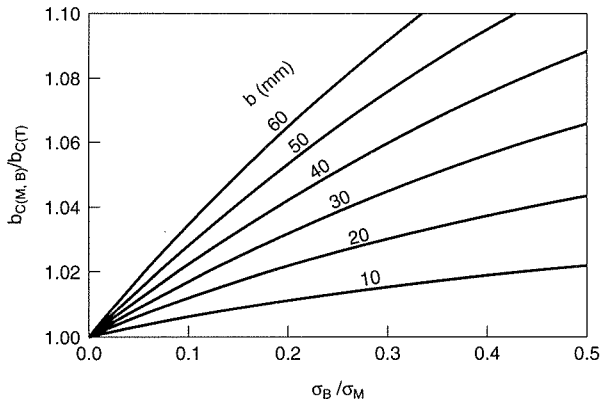

Fig. 28 Correction value of critical surface flaw depth under tension and bending

to the logarithm of stress intensity rate. The upper shelf fracture toughness increased with increasing stress intensity rate. Graphite internodule spacing or nodule size had little effect on dynamic fracture toughness although static fracture toughness was influenced by these factors.

Although unstable fracture can be readily estimate on the basis of linear fracture mechanics using converted plane strain fracture toughness, for more accurate analysis, it is preferable to estimate the propagation of crack by a computer on the basis of nonlinear fracture mechanics.

Acknowledgements

A part of this study was supported by the atomic research fund from Science and Technology Agency in Japan. The author wishes to express his thanks to all those concerned. He also wishes to express his thanks to his colleagues, especially Messrs. K. Nakano, N. Iwao and N. Furuya, who contributed to the performance of the experimental work. The author is much indebted to Kubota Ltd. for the help in preparing the material.

References

1) W.L. Bradley and M.N. Srinivasan: Int. Mater. Rev., **35** (1990), 129–161.
2) H. Mayer: AFS Int. Cast Met. J., **1** (1976), 21–27.
3) W.L. Bradley: J. Met., **37**, No. 1 (1985), 74–76.
4) S. Nakamura, N. Sakamoto, K. Inoue, K. Ōgi and K. Matsuda: J. Jpn. Found. Soc., **59** (1987), 664–669.
5) T. Yanaka, H. Saito, D. Sakurai and H. Arata: J. Jpn. Found. Soc., **60** (1988), 20–25.
6) Y. Iwabuchi, H. Narita, M. Murata, S. Shimizu and O. Tsumura: J. Jpn. Found. Soc., **60** (1988), 167–172.
7) JIS G 5504, Heavy-walled Ferritic Spheroidal Graphite Iron Castings for Low Temperature Service
8) R.K. Nanstad, F.J. Worzala and C.R. Loper, Jr.: Int. Symp. Met. Cast Iron, **2** (1975), 789–807.
9) R.K. Nanstad, F.J. Worzala and C.R. Loper, Jr: Trans. Am. Foundrymen Soc., **83** (1975), 245–256.
10) F.J. Worzala, R.W. Heine and Yi Wen Cheng: Trans. Am. Foundrymen Soc., **84** (1976), 675–682.
11) Yi-W. Cheng and F.J. Worzala: Int. Conf. Mech. Behav. Mater., **2** (1976), 1223–1227.
12) B. Ostensson: Scand. J. Met., **2** (1973), 194–196.
13) T. Arai, T. Onchi, T. Saegusa and G. Yagawa: Proceedings the 6th Sympo. Fract. and Fract. Mech., Soc. Mat. Sci. Jpn, (1991), 99–104.
14) W.L. Bradley and H.E. Mead, Jr.: ASME MPC, **11** (1979), 69–87.
15) W.L. Bradley: Trans. Am. Foundrymen Soc., **89** (1981), 837–848.
16) S.R. Holdsworth and G. Jolley: Int. Symp. Met. Cast Iron, (1975), 809–825.
17) T. Maezono, Y. Ohtsuka, R. Takahashi, M. Yano and Y. Ishihara: J. Jpn. Found. Soc., **58** (1986), 195–199.
18) S. Komatsu, T. Shiota and K. Nakamura: J. Jpn. Found. Soc., **60** (1988), 442–447.
19) S. Komatsu, T. Shiota and K. Nakamura: J. Jpn. Found. Soc., **59** (1987), 554–559.
20) A.J. Krasowsky, I.V. Kramarenko and V.V. Kalaida: Fatigue Fract. Eng. Mater. Struct., **10** (1987), 223–237.
21) T. Kobayashi: Casting & Forging, **30**, No.7 (1977), 5–12.
22) F. Henke: Giesserei Prax., No. 9/10 (1976), 131–139.
23) S. Komatsu, T. Shiota and K. Nakamura: J. Jpn. Found. Soc., **60** (1988), 643–648.
24) K. Kuribayashi, T. Kishi, P. Bhandhubanyong, M. Ito, T. Umeda and Y. Kimura: Tetsu-to-Hagame, **60** (1983), 663–670.
25) S. Komatsu, T. Shiota and K. Nakamura: J. Jpn. Found. Soc., **59** (1987), 159–163.

26) K.B. Sorenson and R. Salzbrenner: "The Mechanism of Fracture," ed. by Goel, ASM, (1986), 415–419.
27) T. Maezono, R. Takahashi and M. Suenaga: J. Jpn. Found. Soc., **60** (1988), 578–583.
28) R. Salzbrenner: J. Mater. Sci., **22** (1987), 2135–2147.
29) Y. Iwabuchi, H. Narita and O.Tsumura: J. Jpn. Found. Soc., **60** (1988), 215–220.
30) T. Kobayashi and S. Nishi: J. Jpn. Found. Soc., **52** (1980), 76–87, (Communication paper for the 46th Int. Foundry Congr., Madrid, Spain).
31) T. Luyendijk and H. Nieswaag: Int. Foundry Congr., (1982), 1–13.
32) T. Kobayashi, H. Yamamoto and K. Matsuo: Eng. Fract. Mech., **30** (1988), 397–407.
33) "Research on Quality Assurance of Ductile Cast Iron Casks," Quality Assurance Committee on Ductile Cast Iron Casks, CRIEPI Report, (1990).
34) E. Fujii, Y. Sakai and Y. Ando: J. Tes. Eval., **14** (1986), 181–190.
35) T. Kobayashi, I. Yamamoto and M. Niinomi: Eng. Fract. Mech., **24** (1986), 773–782.
36) A.K. Shoemaker and S.T. Rolfe: Eng. Fract. Mech., **2** (1971), 319–339.
37) W.N. Sharpe, Jr. and J.M. Shapiro: J. Test. Eval., **18** (1990), 38–44.
38) M.R. Bayoumi, J.R. Klepaczko and M.N. Bassim: J. Test. Eval., **12** (1984) 316–323.
39) K. Hirano, H. Kobayashi and H. Nakazawa: J. Test. Eval., **13** (1985), 356–362.
40) J.R. Joyce and C.S. Schneider: J. Test. Eval., **16** (1988), 257–270.
41) J.F. Kalthoff: Int. J. Fract., **27** (1985), 277–298.
42) ASTM Standard E813-81, Standard Test for J_{IC}
43) ASTM Standard E813-87, Standard Test for J_{IC}
44) British Standard Method 7448 (1991), Fracture Mechanics, Toughness Tests, Part 1.
45) M.W. Schwartz and L. Boyce: "Ductile and Brittle Failure Design Criteria for Nodular Cast Iron Spent-Fuel Shipping Containers," US DOE Rep., UCRL-53046, (1983).
46) M. Ishida, H. Noguchi and T. Yoshida: Int. J. Fract., **26** (1984), 157–188.
47) T. Yasunaka, K. Nakano and T. Saito: ISIJ International, **31** (1991), 298–303.
48) T. Yasunaka, N. Iwao, N. Furuya, H. Yamawaki, S. Matsumoto and K. Kimura: Tetsu-to-Hagane, **71** (1985), 1398–1404.
49) T. Yasunaka, N. Iwao, N. Furuya, K. Kimura and H. Yamawaki: J. Soc. Mater. Sci. Jpn., **33** (1984), 1336–1341.
50) K. Nakano and T. Yasunaka: Tetsu-to-Hagane, **78** (1992), 926–993.
51) T. Yasunaka and K. Nakano: Proc. the 10th Int. Symp. Packaging and Transportation of Radioactive Materials, (1992), 1304–1310.
52) K. Nakano and T. Yasunaka: Tetsu-to-Hagane, **80** (1994), 330–335.

Dynamic Fracture Toughness and Its Evaluation in
a Heavy-Sectioned Ferritic Nodular Cast Iron

by

Takashi YASUNAKA

NRIM Special Report
(Research Report)
No. 94-02

Date of issue: 31 March, 1994

Publisher, Contact:
Toshikazu ISHII
Planning Section, Administration Division
National Research Institute for Metals
2–3–12, Nakameguro, Meguro-ku, Tokyo 153, Japan
Phone: +81-3-3719-2271 Fax: +81-3-3792-3337

Typeset using the SGML by Uniscope, Inc., Tokyo

Dynamic Fracture Toughness and Its Evaluation in a Heavy-Sectioned Ferritic Nodular Cast Iron

by

Takashi YASUNAKA

NRIM Special Report
(Research Report)
No. 94–02

Contents